Front. Phys., 2014, 9(6): 698–710
DOI 10.1007/s11467-013-0361-5

REVIEW ARTICLE

Time-dependent density functional theory for quantum transport

Yanho Kwok, Yu Zhang, GuanHua Chen†

Department of Chemistry, The University of Hong Kong, Hong Kong, China

E-mail: †ghc@everest.hku.hk

Received March 31, 2013; accepted June 15, 2013

The rapid miniaturization of electronic devices motivates research interests in quantum transport. Recently time-dependent quantum transport has become an important research topic. Here we review recent progresses in the development of time-dependent density-functional theory for quantum transport including the theoretical foundation and numerical algorithms. In particular, the reduced-single electron density matrix based hierarchical equation of motion, which can be derived from Liouville–von Neumann equation, is reviewed in details. The numerical implementation is discussed and simulation results of realistic devices will be given.

Keywords tim-dependent density functional theory (TDDFT), quantum transport, nonequilibrium Green's function

PACS numbers 71.15.Mb, 72.10.Bg, 73.23.Ad, 73.63.-b

Contents

1 Introduction

Given the rapid miniaturization of electronic devices [1] down to nanometer scale, whether it is possible to construct electronic devices from individual molecules becomes a natural and important question. Molecular electronics, which either refer to molecular materials for electronics in the top-down approach or electronics constructed with single molecule in the bottom-up approach [2], have become an active research area in both fundamental science as well as technological application point of view. The idea of building electronics with single molecule is not new and can be dated back to the 1970s [3]. And great progress has been achieved throughout the last decades [4–12].

On the experimental side, the advance in nanofabrication techniques allows the realization of molecular junction such that current through a single molecule can be measured. And recent advancement has been made in measuring the transient current of quantum dots [13].

On the theoretical side, the Landauer–Büttiker formalism has become a standard and routine approach to study the steady state current through the molecular devices. Combined with effective single particle theory such as density functional theory (DFT) and Keldysh's nonequilibrium Green's function (NEGF) formalism, namely DFT-NEGF method, we can carry out first-principles simulation of molecular devices composed of hundreds of atoms readily to study their steady state properties [14, 15]. If larger scale simulation is desirable, one can turn to empirical method such as tight binding method or density-functional tight-binding (DFTB) method [16, 17], which is a tight binding method parameterized with DFT calculation. If we would like to simulate even larger systems or include the effect of surrounding substrate into simulation, we can apply multi-scale quantum mechanics and electromagnetics (QM/EM) simulation [18, 19]. In this case, QM method is applied for the molecu-

lar device region in which quantum effect is critical and classical EM method is used to describe the surrounding less important environment.

This review, however, will focus on simulation of time-domain quantum transport phenomena of molecular devices [20–29], in contrast to the energy domain steady state simulation mentioned above. Currently, time domain simulation is still a difficult and challenging area to be explored. Time domain simulation is of interest for a couple of reasons [30]. First, it allows us to follow the real time evolution of the system of interest under a time dependent bias voltage. We can then study the transient dynamics of the system, determine the switch-on time for devices and study how the current develops through the molecules after the voltage is turned on. We can also use it to study the AC response as well as response under any kinds of signal voltages since time-dependent simulation includes full frequency information [31]. Last but not least, the achievement of steady state is not guaranteed [32–35]. It has been shown that the presence of multiple bound states in the system can lead to non-decaying oscillating current, of which the amplitude depends on the entire history of the applied voltage and can be larger than the steady state current [33, 34].

This review is organized as follows. First of all, we will give a brief introduction on how we model the quantum transport problem as well as the NEGF formalism. Second, we will talk about combining TDDFT and NEGF and the theoretical bases behind this. Third, an exact time-dependent density functional theory (TDDFT) for quantum transport as well as practical numerical schemes are reviewed. Finally, an efficient computational scheme based on the commonly used wide-band limit (WBL) approximation is presented and numerical implements are demonstrated.

2 Modeling the problem and NEGF formalism

The typical experimental set-up measuring current through molecular devices is shown in the schematic diagram (Fig. 1).

Modeling this experimental set-up is a difficult multi-scale problem since we have a microscopic molecule connected to macroscopic electrodes, wires and power source. The common approach to model it is to partition the entire system into device and leads regions, as shown in Fig. 2. The central device region contains the molecular device of interest contacted with few atomic layers of the electrodes. This is the region where scattering takes place and thus the region we are interested in. Connected to the device region are the left and right lead regions, which act as electron reservoirs. Before switching on the voltage, the entire system is in equilibrium, sharing the same temperature and chemical potential. The application of bias voltage then shifts the Hamiltonian and chemical potential in the leads, creates an electric field in the device region and results in current flowing from higher chemical potential side to lower side.

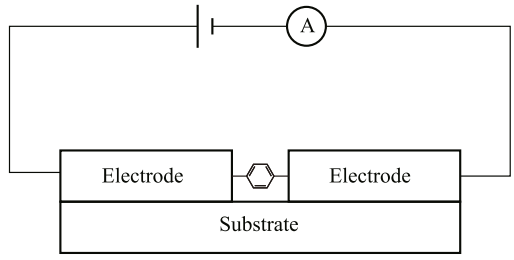

Fig. 1 Schematic diagram showing the experimental set-up for measuring current through molecular devices.

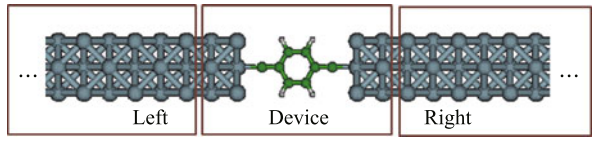

Fig. 2 Schematic diagram showing the partitioning of entire system into device and lead regions.

Now we come to the question how to treat the macroscopic leads properly. Early approaches ignore the lead region and simulate a finite system consisting of the device contacted with a few layers of the electrodes [36, 37]. To prevent the back reflection from the lead boundary, complex absorbing potentials (CAP) is applied at the end of the finite leads to remove electrons reaching the edges [38, 39]. Another approach is the Landauer-Büttiker approach. In this approach, we assume the electrodes extend semi-infinitely in the transport direction. With the Keldysh NEGF Formalism, we can treat the effect of the semi-infinite electrodes properly. Here we will give a brief review on it. Readers who are not familiar with the Keldysh NEGF Formalism are referred to Ref. [12] for more details.

Suppose our system is real space discretized or expanded by some orthonormal localized basis. Our system Hamiltonian can then be arranged and partitioned into the following form:

$$\boldsymbol{H} = \begin{pmatrix} \boldsymbol{H}_{LL} & \boldsymbol{H}_{LD} & \mathbf{0} \\ \boldsymbol{H}_{DL} & \boldsymbol{H}_{DD} & H_{\boldsymbol{D}R} \\ \mathbf{0} & \boldsymbol{H}_{RD} & \boldsymbol{H}_{RR} \end{pmatrix} \tag{1}$$

where the diagonal block matrices $\boldsymbol{H}_{LL}, \boldsymbol{H}_{DD}, \boldsymbol{H}_{RR}$ are the Hamiltonian projected onto the left lead, central de-

vice and right lead regions respectively. The off-diagonal hopping matrices $\boldsymbol{H}_{LD} = \boldsymbol{H}_{DL}^{\dagger}, \boldsymbol{H}_{RD} = \boldsymbol{H}_{DR}^{\dagger}$ represent the coupling between leads and device region. The retarded Green's function is then defined as

$$\left[\mathrm{i}\frac{\partial}{\partial t} - \boldsymbol{H}(t)\right]\boldsymbol{G}^{r}(t,t') = \delta(t-t')\boldsymbol{I} \tag{2}$$

which can be partitioned similarly as

$$\boldsymbol{G}^{r} = \begin{pmatrix} \boldsymbol{G}_{L}^{r} & \boldsymbol{G}_{LD}^{r} & \boldsymbol{G}_{LR}^{r} \\ \boldsymbol{G}_{DL}^{r} & \boldsymbol{G}_{D}^{r} & \boldsymbol{G}_{DR}^{r} \\ \boldsymbol{G}_{RL}^{r} & \boldsymbol{G}_{RD}^{r} & \boldsymbol{G}_{R}^{r} \end{pmatrix} \tag{3}$$

If the coupling between the device region and lead regions are neglected, i.e., the off-diagonal term in Eq. (1) is neglected, the bare Green's functions $\boldsymbol{g}_{i}^{r}(t,t')$ can be defined for each region as

$$\left(\mathrm{i}\frac{\partial}{\partial t} - \boldsymbol{H}_{ii}\right)\boldsymbol{g}_{i}^{r}(t,t') = \delta(t-t')\boldsymbol{I} \tag{4}$$

where $i = L, D, R$. With the coupling between device and leads treated as perturbation, Dyson's equation is derived to evaluate the Green's function $\boldsymbol{G}(t,t')$ from the bare Green's function $g(t,t')$ and coupling matrix $\boldsymbol{V}$, $\boldsymbol{G}(t,t') = \boldsymbol{g}(t,t') + \int_{-\infty}^{\infty}\mathrm{d}\tau\boldsymbol{g}(t,\tau)\boldsymbol{V}(\tau)\boldsymbol{G}(\tau,t')$, where

$$\boldsymbol{V} = \begin{pmatrix} \boldsymbol{0} & \boldsymbol{H}_{LD} & \boldsymbol{0} \\ \boldsymbol{H}_{DL} & \boldsymbol{0} & \boldsymbol{H}_{DR} \\ \boldsymbol{0} & \boldsymbol{H}_{RD} & \boldsymbol{0} \end{pmatrix} \tag{5}$$

Hence, Dyson equation for device retarded Green's function is obtained as

$$\boldsymbol{G}_{D}^{r}(t,t') = \boldsymbol{g}_{D}^{r}(t,t') + \sum_{\alpha=L,R}\int_{-\infty}^{\infty}\mathrm{d}\tau_1\mathrm{d}\tau_2\boldsymbol{g}_{D}^{r}(t,\tau_1)\boldsymbol{\Sigma}_{\alpha}^{r}(\tau_1,\tau_2)\boldsymbol{G}_{D}^{r}(\tau_2,t') \tag{6}$$

where $\boldsymbol{\Sigma}_{\alpha}^{r}(\tau_1,\tau_2) = \boldsymbol{h}_{D\alpha}\boldsymbol{g}_{\alpha}^{r}(\tau_1,\tau_2)\boldsymbol{h}_{\alpha D}$ is the self-energy accounting for the coupling between device and lead α. The real part of self-energy describes the energy level shifting while its imaginary part gives the level broadening, accounting for the finite life time of electrons entering and leaving the device region. With the Langreth Rules for analytic continuation, the Dyson's equation for the device advanced, lesser and greater Green's function can be obtained similarly:

$$\boldsymbol{G}_{D}^{a}(t,t') = \boldsymbol{g}_{D}^{a}(t,t') + \sum_{\alpha=L,R}\int_{-\infty}^{\infty}\mathrm{d}\tau_1\mathrm{d}\tau_2\boldsymbol{g}_{D}^{a}(t,\tau_1)\boldsymbol{\Sigma}_{\alpha}^{a}(\tau_1,\tau_2)\boldsymbol{G}_{D}^{a}(\tau_2,t') \tag{7}$$

$$\begin{aligned}\boldsymbol{G}_{D}^{>,<}(t,t') = \boldsymbol{g}_{D}^{>,<}(t,t') + \sum_{\alpha=L,R}\int_{-\infty}^{\infty}\mathrm{d}\tau_1\mathrm{d}\tau_2[&\boldsymbol{g}_{D}^{r}(t,\tau_1)\boldsymbol{\Sigma}_{\alpha}^{r}(\tau_1,\tau_2)\boldsymbol{G}_{D}^{>,<}(\tau_2,t') \\ &+\boldsymbol{g}_{D}^{>,<}(t,\tau_1)\boldsymbol{\Sigma}_{\alpha}^{a}(\tau_1,\tau_2)\boldsymbol{G}_{D}^{a}(\tau_2,t') + \boldsymbol{g}_{D}^{r}(t,\tau_1)\boldsymbol{\Sigma}_{\alpha}^{>,<}(\tau_1,\tau_2)\boldsymbol{G}_{D}^{a}(\tau_2,t')]\end{aligned} \tag{8}$$

Differentiating the above Dyson equations gives the Kadanoff–Baym equations, the equations of motion of the device Green's functions.

$$\begin{aligned}&\left[\mathrm{i}\frac{\partial}{\partial t} - \boldsymbol{H}_{D}(t)\right]\boldsymbol{G}_{D}^{r/a}(t,t') \\ &\quad= \delta(t-t')\boldsymbol{I} + \int_{-\infty}^{\infty}\mathrm{d}\tau\boldsymbol{\Sigma}_{\alpha}^{r/a}(t,\tau)\boldsymbol{G}_{D}^{r/a}(\tau,t') \\ &\left[\mathrm{i}\frac{\partial}{\partial t} - \boldsymbol{H}_{D}(t)\right]\boldsymbol{G}_{D}^{>/<}(t,t') \\ &\quad= \int_{-\infty}^{\infty}\mathrm{d}\tau[\boldsymbol{\Sigma}_{\alpha}^{r}(t,\tau)\boldsymbol{G}_{D}^{>/<}(\tau,t') \\ &\qquad+\boldsymbol{\Sigma}_{\alpha}^{>/<}(t,\tau)\boldsymbol{G}_{D}^{a}(\tau,t')]\end{aligned} \tag{9}$$

The Kadanoff–Baym equations determine the real-time evolution of the device region we are interested in. However, the initial values of the Green's functions need to be determined from the Dyson equations.

3 Time dependent density functional theory

As mentioned, atomistic first-principles simulations of molecular devices are useful in interpreting experimental results as well as giving prediction. DFT or TDDFT is probably the most commonly used method given its good accuracy and relatively small computational cost.

The theoretical foundation for density functional theory lies in the Hohenberg–Kohn (HK) theorem [40] which states that the ground state electron-density function determines uniquely the external potential and thus all electronic properties of the system. Similarly, the TDDFT is based on Runge–Gross theorem which shows that time-dependent electron density $\rho(t)$ determines the electronic properties of a time-dependent system [41]. Following the suggestion by Kohn and Sham, instead of the original many-body interacting system, it is able to simulate an effective non-interacting reference system with a carefully chosen Hamiltonian such that it reproduces exactly the same electron density $\rho(t)$ as the original system. From the correct electron density, all the electronic properties of interest are then determined. The effective Kohn–Sham (KS) reference system Hamiltonian is given by

$$H(t) = \sum_{i=1}^{N} h(\boldsymbol{r}_i, t) = \sum_{i=1}^{N} \left[-\frac{1}{2}\nabla_i{}^2 + \upsilon_{KS}(\boldsymbol{r}_i, t) \right] \quad (10)$$

where $\upsilon_{KS}(\boldsymbol{r}, t) = \upsilon_{ext}(\boldsymbol{r}, t) + \upsilon_H(\boldsymbol{r}, t) + \upsilon_{xc}(\boldsymbol{r}, t)$ is the effective KS potential which comprises of external potential, mean field electron–electron repulsion as well as exchange–correlation (XC) potential. If the exact XC functional is available, this reference system in principle will evolve in a way that produces the exact electron density.

However, it should be noted that while the above two theorems are applicable only for isolated or closed system, the device region we are talking about is indeed an open system since electrons can enter and leave the region. Extending DFT or TDDFT to open system then relies on the so called holographic electron density theorem (HEDT). In 2004, Fournais *et al.* [42, 43] first proved the analyticity of time-independent the electron density of any real physical systems made of atoms and molecules. The analyticity of electron density means that given a piece of electron density on a finite subspace, we can in principle do analytical continuation to obtain the electron density on the entire system. Thus the finite piece of electron density in the device region determines the electronic properties of the entire system. It is known as the holographic electron density theorem (HEDT) which forms the foundation for DFT for open system.

And in 2007, Chen *et al.* extended the HEDT to time-dependent case [24]. They proved that if the initial (at $t = t_0$) electron density $\rho(r, t_0)$ as well as the time-dependent external potential $\upsilon(r, t)$ are real analytic in real space, then the electron density on any finite subsystem at any time $\rho_D(r, t)$ determines uniquely the electron density of whole system. This means that in principle we can extract all electronic properties of the system from the electron density within the device region. This time-dependent holographic electron density theorem (TD-HEDT) proves the existence of TDDFT method for open system and provides a legitimate for us to combine TDDFT and NEGF formalism [24, 44]. If current density is employed as the basic physical quantity of interest, the extension of time-dependent current-density functional theory (TDCDFT) [45] to open quantum system was rigorously established, which was termed as stochastic TDCDFT [46, 47].

In the TDDFT-NEGF formalism, we can solve the Dyson equation or the Kadanoff–Baym equations with the KS time-dependent Hamiltonian $h(t) = -\frac{1}{2}\nabla^2 + \upsilon_{KS}(\boldsymbol{r}, t)$. It is noted that within the TDDFT formalism, all many body effects are in principle included in the XC potential in this single particle Hamiltonian which is local in both time and space.

4 TDDFT-NEGF formalism

The first computational scheme which combines TDDFT and NEGF to simulate transient response with the infinite leads set-up was suggested by Kurth *et al.* [22]. Instead of the Kadanoff–Baym equations, they partition time-dependent Schrodinger equation into leads and device region and derive the Schrodinger equation for the projected wave function onto device region,

$$\mathrm{i}\frac{\partial}{\partial t}\psi_D(t) = \boldsymbol{H}_D(t)\psi_D(t) + \mathrm{i}\sum_{\alpha} \boldsymbol{H}_{D\alpha}\boldsymbol{g}(t, t_0)\psi_\alpha(t_0) + \sum_{\alpha}\int_{t_0}^{t} \mathrm{d}t' \boldsymbol{\Sigma}_\alpha(t, t')\psi_D(t') \quad (11)$$

The second last term is called the source term describing the injection of electron from leads into the device region. The last term corresponds to the so called memory term since it involves a time integral of the past history from t_0 to t. Practically, they integrate the time-dependent Schrodinger equation and replace the propagator $\exp(-\mathrm{i}H\Delta t)$ by a finite difference representation known as Cayley's form.

$$\exp(-\mathrm{i}\boldsymbol{H}\Delta t) = \frac{1 - \mathrm{i}\frac{\Delta t}{2}\boldsymbol{H}}{1 + \mathrm{i}\frac{\Delta t}{2}\boldsymbol{H}} + O(\Delta t^2) \quad (12)$$

A discretized version which propagates ψ_D from the mth time step to the $m+1$th time step is then as follows:

$$\psi_D^{(m+1)} = \frac{1 - \mathrm{i}\boldsymbol{H}_{eff}^{(m)}\frac{\Delta t}{2}}{1 + \mathrm{i}\boldsymbol{H}_{eff}^{(m)}\frac{\Delta t}{2}}\psi_D^{(m)} + \boldsymbol{S}^{(m)} - \boldsymbol{M}^{(m)} \quad (13)$$

where $\boldsymbol{H}_{eff}^{(m)} = \boldsymbol{H}_D^{(m)} - \sum_{\alpha} \mathrm{i}\frac{\Delta t}{2}\boldsymbol{H}_{C\alpha}(1 + \frac{\Delta t}{2}\boldsymbol{H}_{\alpha\alpha})^{-1}\boldsymbol{H}_{\alpha D}$ is the effective Hamiltonian for the device region, with $\boldsymbol{H}^{(m)} = \frac{1}{2}[\boldsymbol{H}(t_{m+1}) + \boldsymbol{H}(t_m)]$. The source term $S^{(m)}$ corresponds to second last term in Eq. (11), while the memory term $M^{(m)}$ corresponds to the last term in Eq. (11). The above equation is accurate up to second order and is norm-conserving, which means that it is not necessary to normalize the wavefunction at each time step. With proper transparent boundary condition, the above equation can be propagated to obtain time-dependent KS wavefunction for device region.

There are many works in combining TDDFT and NEGF formalism afterwards. In 2007, Chen *et al.* proved the HEDT for time-dependent system, thus validate the idea of extending TDDFT formalism to open system [24]. They proposed two approximated numerical schemes, the second order approximation and the adiabatic wide-band limit (AWBL) approximation, to simulate the transient current through some more realistic molecular de-

vices such as a graphene-alkene-graphene system. Under the AWBL approximation, the self-energy is assumed to be independent of energy and the memory part is integrated by using adiabatic approximation. In this case, the energy structures of the leads are ignored. There are also other schemes which include, for instance, solving directly the double time-integral Dyson equation [26], solving the Kadanoff–Baym equations [48–51] and the KS Master Equation approach [23, 52].

It is worth mentioning that solving the time-dependent transport problem without approximation on energy structure of leads, such as the WBL approximation, is a difficult and very computationally expensive task. The major difficulty lies in the memory term. It involves a time integral of the past history from initial time t_0 to the current time step t, which is unavoidable whichever scheme you choose and this makes the computational cost scale super-linearly with the total simulation time. In fact, a simple implementation will result in computational cost scaling as $O(t_s^3)$, where t_s is the total simulation time.

In an attempt to reduce the computational complexity with respect to the simulation time, Wang *et al.* develop a method to reduce the complexity from $O(t_s^3)$ to $O(t_s^2 \log^2(t_s))$ [50]. To achieve this, they have to avoid solving Poisson equation at each time step self-consistently from the electron density for the coulomb potential and assume that the coulomb potential immediately reaches the steady state value after switching on the step-like bias voltage. Then they employed fast Fourier transform (FFT) techniques in propagating the Kadanoff-Baym equation for the retarded device Green's function, achieving an $O(t_s^2 \log^2(t_s))$ scaling.

In the following section, we will focus on a particular approach: the reduced single electron density matrix (RSDM) based hierarchical equation of motion (HEOM) approach, which is able to achieve linear scaling over simulation time. And some numerical results of TDDFT simulation of quantum transport in molecular devices will be reviewed.

5 Reduced single electron density matrix based hierarchical equation of motion approach

The RSDM based HEOM approach originates from the Liouville–von Neumann equation [25]. In this approach, the basic variable is the RSDM instead of the KS orbitals. The Liouville–von Neumann equation for the RSDM of device region with the electronic degrees of freedom of the electrodes projected out is known as

$$\mathrm{i}\frac{\mathrm{d}}{\mathrm{d}t}\boldsymbol{\sigma}_D(t) = [\boldsymbol{h}_D, \boldsymbol{\sigma}_D] - \mathrm{i}\sum_\alpha \boldsymbol{Q}_\alpha(t) \tag{14}$$

where $\boldsymbol{\sigma}_D(t)$ is the RSDM for device region and is equivalent to the lesser Green's function at $t = t'$ [$\boldsymbol{\sigma}_D(t) = -\mathrm{i}\boldsymbol{G}_D^<(t,t)$] in NEGF language. $\boldsymbol{Q}_\alpha(t) = \mathrm{i}\,[\boldsymbol{h}_{D\alpha}\boldsymbol{\sigma}_{\alpha D} - \boldsymbol{\sigma}_{D\alpha}\boldsymbol{h}_{\alpha D}]$ is known as the dissipative term between device and lead α. In NEGF formalism, it can be expressed as

$$\begin{aligned}\boldsymbol{Q}_\alpha(t) = \int_{-\infty}^{\infty} \mathrm{d}\tau [&\boldsymbol{\Sigma}_\alpha^r(t,\tau)\boldsymbol{G}_D^<(\tau,t) \\ &+\boldsymbol{\Sigma}_\alpha^<(t,\tau)\boldsymbol{G}_D^a(\tau,t) + H.c.]\end{aligned} \tag{15}$$

The trace of $\boldsymbol{Q}_\alpha(t)$ gives time-dependent electric current passing from lead α into the device region,

$$J_\alpha(t) = -e\frac{\mathrm{d}}{\mathrm{d}t}\int_\alpha \mathrm{d}\boldsymbol{r}\rho(\boldsymbol{r},t) = -e\ \mathrm{Tr}[\boldsymbol{Q}_\alpha(t)] \tag{16}$$

Given the TD-HEDT, Eq. (14) is in principle a closed equation of motion for RSDM since the KS Hamiltonian $h_D(t)$ and the dissipative term $Q_\alpha(t)$ are both functionals of electron density $\sigma_D(t)$ in device region according to HEDT. In practice, instead of evaluating $Q_\alpha(t)$ from its definition and propagate Eq. (14), a hierarchical equation of motion is derived and propagated instead. The HEOM is known as follows [25]:

$$\begin{aligned}
&\mathrm{i}\dot{\boldsymbol{\sigma}}_D(t) = [\boldsymbol{h}_D, \boldsymbol{\sigma}_D] - \sum_\alpha \int \mathrm{d}\varepsilon \left[\boldsymbol{\varphi}_\alpha(\varepsilon,t) - \boldsymbol{\varphi}_\alpha{}^\dagger(\varepsilon,t)\right] \\
&\mathrm{i}\dot{\boldsymbol{\varphi}}_\alpha(\varepsilon,t) = [\boldsymbol{h}_D(t) - \varepsilon - \Delta_\alpha]\,\boldsymbol{\varphi}_\alpha(\varepsilon,t) + [f_\alpha(\varepsilon) \\
&\qquad -\boldsymbol{\sigma}_D]\boldsymbol{\Lambda}_\alpha(\varepsilon) + \sum_{\alpha'}\int \mathrm{d}\varepsilon'\ \boldsymbol{\varphi}_{\alpha,\alpha'}(\varepsilon,\varepsilon',t) \\
&\mathrm{i}\dot{\boldsymbol{\varphi}}_{\alpha,\alpha'}(\varepsilon,\varepsilon',t) \\
&\quad = [\varepsilon' + \Delta_{\alpha'}(t) - \varepsilon - \Delta_\alpha(t)]\,\boldsymbol{\varphi}_{\alpha,\alpha'}(\varepsilon,\varepsilon',t) \\
&\qquad +\boldsymbol{\Lambda}_{\alpha'}(\varepsilon')\boldsymbol{\varphi}_\alpha(\varepsilon,t) - \boldsymbol{\varphi}_{\alpha'}^\dagger(\varepsilon',t)\boldsymbol{\Lambda}_\alpha(\varepsilon)
\end{aligned} \tag{17}$$

where $\boldsymbol{\varphi}_\alpha(\varepsilon,t)$ and $\boldsymbol{\varphi}_{\alpha,\alpha'}(\varepsilon,\varepsilon',t)$ are known as the 1st and 2nd tier auxiliary reduced-single electron density matrices (ARSDM) defined by

$$\begin{aligned}
&\boldsymbol{\varphi}_\alpha(\epsilon,t) = -\mathrm{i}\left[\int_C \mathrm{d}\tau \boldsymbol{G}_D(t,\tau)\boldsymbol{\Sigma}_\alpha(\epsilon;\tau,t)\right]^< = \mathrm{i}\int_{-\infty}^t \mathrm{d}\tau\left[\boldsymbol{G}_D^<(t,\tau)\boldsymbol{\Sigma}_\alpha^>(\epsilon;\tau,t) - \boldsymbol{G}_D^>(t,\tau)\boldsymbol{\Sigma}_\alpha^<(\epsilon;\tau,t)\right] \\
&\boldsymbol{\varphi}_{\alpha,\alpha'}(\epsilon,\epsilon',t) = \mathrm{i}\left[\int_C \mathrm{d}\tau_1 \int_C \mathrm{d}\tau_2 \boldsymbol{\Sigma}_{\alpha'}(\epsilon';t,\tau_1)\boldsymbol{G}_D(\tau_1,\tau_2)\boldsymbol{\Sigma}_\alpha(\epsilon;\tau_2,t)\right]^<
\end{aligned} \tag{18}$$

A comparison with Eq. (14) gives $\boldsymbol{Q}_\alpha(t)$ in terms of $\boldsymbol{\varphi}_\alpha(\varepsilon,t)$:

$$\boldsymbol{Q}_\alpha(t) = -\mathrm{i}\int \mathrm{d}\varepsilon \left[\boldsymbol{\varphi}_\alpha(\varepsilon,t) - \boldsymbol{\varphi}_\alpha{}^\dagger(\varepsilon,t)\right] \tag{19}$$

The above HEOM can be derived easily with the help of NEGF formalism, by differentiating the Eq. (18) and applying the equation of motion for device lesser/greater Green's function $\boldsymbol{G}_D^{>/<}(t,t')$ and the equation of motion of energy dispersed self-energy $\boldsymbol{\Sigma}_\alpha^{>/<}(\varepsilon,\tau,t)$:

$$\begin{aligned}
&\mathrm{i}\frac{\partial}{\partial t}\boldsymbol{G}_D^<(t,t') = \boldsymbol{h}_D(t)\boldsymbol{G}_D^<(t,t') \\
&+\sum_\alpha \int_{-\infty}^{\infty} \mathrm{d}\tau[\boldsymbol{\Sigma}_\alpha^r(t,\tau)\boldsymbol{G}_D^<(\tau,t') + \boldsymbol{\Sigma}_\alpha^<(t,\tau)\boldsymbol{G}_D^a(\tau,t')] \\
&\mathrm{i}\frac{\partial}{\partial t}\boldsymbol{\Sigma}_\alpha^{<,>}(\epsilon,t,t') = [\epsilon+\Delta_\alpha(t)]\,\boldsymbol{\Sigma}_\alpha^{<,>}(\epsilon,t,t')
\end{aligned} \tag{20}$$

It is noted that unlike the HEOM for reduced (many-electron) density matrix, which has infinitely many tiers [53], the HEOM for reduced single-electron density matrix within TDDFT scheme is closed exactly at the second tier. This is a consequence of the non-interacting nature of KS reference system in TDDFT formalism. The RSDM based HEOM is thus expected to be a computationally efficient and in principle exact approach within the TDDFT-NEGF formalism.

5.1 Numerical implementation

In practical implementation, efficient ways have to be found to evaluate energy-integral in the HEOM, which means to convert the integral into a summation. Two decomposition schemes have been proposed and applied to tight-binding model calculation. One is the Chebyshev decomposition scheme [54], which is an accurate scheme and is applicable to both finite and zero temperature, though it can be computationally expensive since the number of expansion terms is directly proportional to the simulation time. Another approach is the Lorentzian–Padé decomposition scheme [55], which is an approximated scheme beyond WBL approximation. It involves approximating the line-width function $\boldsymbol{\Lambda}_\alpha(E) = \mathrm{i}\left[\boldsymbol{\Sigma}_\alpha^r(E) - \boldsymbol{\Sigma}_\alpha^a(E)\right]$ by a summation of Lorentzian functions and decompose the Fermi–Dirac distribution by Padé spectrum decomposition [56]:

$$\boldsymbol{\Lambda}_\alpha(\epsilon) \approx \sum_{d=1}^{N_d} \frac{{w_d}^2}{(\epsilon-\Omega_d)^2+{w_d}^2}\bar{\boldsymbol{\Lambda}}_{\alpha,d} \tag{21}$$

$$f(\epsilon-\mu) \approx \frac{1}{2} - \sum_p \left(\frac{R_p}{\epsilon-\mu+\mathrm{i}z_p} + \frac{R_p}{\epsilon-\mu-\mathrm{i}z_p}\right) \tag{22}$$

In this case, the lesser self-energy in time domain can be evaluated analytically by Cauchy's residue theorem, resulting in

$$\begin{aligned}
&\boldsymbol{\Sigma}_\alpha^{<,>}(t,t') \\
&= \frac{\mathrm{i}}{2\pi}\int_{-\infty}^{\infty} \mathrm{d}\epsilon\; f_\alpha^{<,>}(\epsilon)\boldsymbol{\Lambda}_\alpha(\epsilon)\mathrm{e}^{\mathrm{i}\epsilon(t'-t)}\mathrm{e}^{\mathrm{i}\int_t^{t'}\mathrm{d}\tau\,\Delta_\alpha(\tau)} \\
&= \sum_k \boldsymbol{A}_{\alpha,k}^{<,>}\mathrm{e}^{\mathrm{i}\epsilon_{\alpha,k}(t'-t)}\mathrm{e}^{\mathrm{i}\int_t^{t'}\mathrm{d}\tau\,\Delta_\alpha(\tau)}
\end{aligned} \tag{23}$$

where $\epsilon_{\alpha,k}$ are the poles of $\boldsymbol{\Lambda}_\alpha(\epsilon)$ and $f_\alpha^{<,>}(\epsilon)$ on the upper half complex plane. For poles of $\boldsymbol{\Lambda}_\alpha(\epsilon)$:

$$\epsilon_{\alpha,d} = \Omega_d + \mathrm{i}W_d \tag{24}$$

$$\boldsymbol{A}_{\alpha,d}^{<,>} = \pm\mathrm{i}\frac{w_d}{2}\bar{\boldsymbol{\Lambda}}_{\alpha d} f^{<,>}(\epsilon_{\alpha,d}-\mu_\alpha) \tag{25}$$

For poles of $f_\alpha^{<,>}(\epsilon)$:

$$\epsilon_{\alpha,p} = \mu_\alpha + \mathrm{i}z_p \tag{26}$$

$$\boldsymbol{A}_{\alpha,p}^{<,>} = R_p\boldsymbol{\Lambda}_\alpha(\epsilon_{\alpha,p}) \tag{27}$$

The energy-resolved self-energy can then be redefined as

$$\boldsymbol{\Sigma}_{\alpha,k}^{<,>}(t,t') = \boldsymbol{A}_{\alpha,k}^{<,>}\mathrm{e}^{\mathrm{i}\epsilon_{\alpha,k}(t'-t)}\mathrm{e}^{\mathrm{i}\int_t^{t'}\mathrm{d}\tau\,\Delta_\alpha(\tau)} \tag{28}$$

The HEOM under the Lorentzian–Padé decomposition scheme is then as follows:

$$\begin{aligned}
&\mathrm{i}\dot{\boldsymbol{\sigma}}_D(t) = [\boldsymbol{h}_D(t),\boldsymbol{\sigma}_D(t)] - \sum_{\alpha,k}\left(\boldsymbol{\varphi}_{\alpha,k}(t) - \boldsymbol{\varphi}_{\alpha,k}{}^\dagger(t)\right) \\
&\mathrm{i}\dot{\boldsymbol{\varphi}}_{\alpha,k}(t) = [\boldsymbol{h}_D(t) - (\epsilon_{\alpha,k}+\Delta_\alpha)]\,\boldsymbol{\varphi}_{\alpha,k}(t) \\
&\qquad -[\mathrm{i}\boldsymbol{A}_{\alpha,k}^< + \boldsymbol{\sigma}_D\boldsymbol{\Lambda}_{\alpha,k}] + \sum_{\alpha'k'}\int \boldsymbol{\varphi}_{\alpha k,\alpha'k'}(t) \\
&\mathrm{i}\dot{\boldsymbol{\varphi}}_{\alpha k,\alpha'k'}(t) \\
&\quad = [\bar{\epsilon}_{\alpha',k'} + \Delta_{\alpha'}(t) - \epsilon_{\alpha,k} - \Delta_\alpha(t)]\,\boldsymbol{\varphi}_{\alpha k,\alpha'k'}(t) \\
&\qquad +\boldsymbol{\Lambda}_{\alpha',k'}\boldsymbol{\varphi}_{\alpha,k}(t) - \boldsymbol{\varphi}_{\alpha',k}^\dagger(t)\boldsymbol{\Lambda}_{\alpha,k}
\end{aligned} \tag{29}$$

where $\boldsymbol{\Lambda}_{\alpha,k} = \mathrm{i}\left(\boldsymbol{A}_{\alpha,k}^> - \boldsymbol{A}_{\alpha,k}^<\right)$ and the summation over k includes all Padé and Lorentzian terms. The major advantage of using the Lorentzian–Padé decomposition scheme is that the computational complexity scales linearly with the simulation time, i.e., $O(t_s)$. The number of ARSDM required depends on the number of Lorenzian function and Padé decomposition which are determined by electronic structures of the electrodes as well as the temperature.

5.2 Tight-binding model simulation

The Lorentzian–Padé decomposition scheme has been applied to simulate the time-dependent transport through a one dimension nearest neighbour tight-binding chain [55] and study how the device-lead coupling will affect the transport properties. Two cases were studied:

strong and weak device-lead coupling as illustrated in Fig. 3. The device region consists of two sites and an electronic temperature of 300 K is used in the simulation. In the good contact case, the lead-device coupling is set at 1.8 eV, slightly less than the coupling inside the device and lead which is 2 eV. In the poor contact case, the lead-device coupling is changed to 0.4 eV. 4 Lorentzian functions are used to fit the line-width function $\boldsymbol{\Lambda}_\alpha(E) = \mathrm{i}[\boldsymbol{\Sigma}^r_\alpha(E) - \boldsymbol{\Sigma}^a_\alpha(E)]$ and 10 terms are used in Padé decomposition of Fermi–Dirac distribution. After the voltage is applied, a linear potential drop in the device region is assumed.

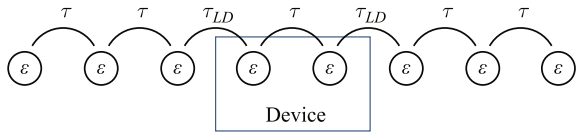

Fig. 3 Nearest neighbour tight-binding model simulated. Good contact: $\tau = 2.0$ eV, $\tau_{LD} = 1.8$ eV; Poor contact: $\tau = 2.0$ eV, $\tau_{LD} = 0.4$ eV.

Figure 4 shows from left to right the I–V characteristics calculated using Landauer formula, the local density of state in the device region in equilibrium state and the time-dependent current respectively. The upper row shows the results for the strong contact case while the lower row is for weak contact case. In both cases, the asymptotic steady state current reached in time-dependent calculation agrees with the prediction of Landauer formula in the I–V curves as it should be. This is because the system here is non-interacting and so the steady state is uniquely determined by the final bias voltage.

For the strong contact case, it can be seen that at small voltages, the I–V curve is linear. But when the voltage is increased further, the I–V curve bends down. This is known as the negative differential resistance (NDR) [57] and is a important feature in semiconductor devices such as resonant tunneling diode. Here, the NDR is due to the finite band width of leads. The current decreases at large voltage because the energy band of the leads is shifted away from the two energy levels in the device. For the transient current, we can see that it reaches the steady state smoothly and rapidly in about 2 femtoseconds(fs).

For the poor contact case, due to the weak coupling to the lead, the line-width function $\boldsymbol{\Lambda}_\alpha(E)$ is small and this results in two sharp peaks in the DOS diagram corresponding to the two energy level in device region. The small peak broadening means that the electrons have long lifetimes inside the device region. In the I–V curve, the current is in general much smaller than that in strong contract case due to the weak coupling. The current shows a sharp increase at 4 V because at that point, the chemical potential of the lead is shifted to align with the energy level in the device. This results in resonant tunneling. The transient current shows large and long lasting oscillation before reaching the steady state. The

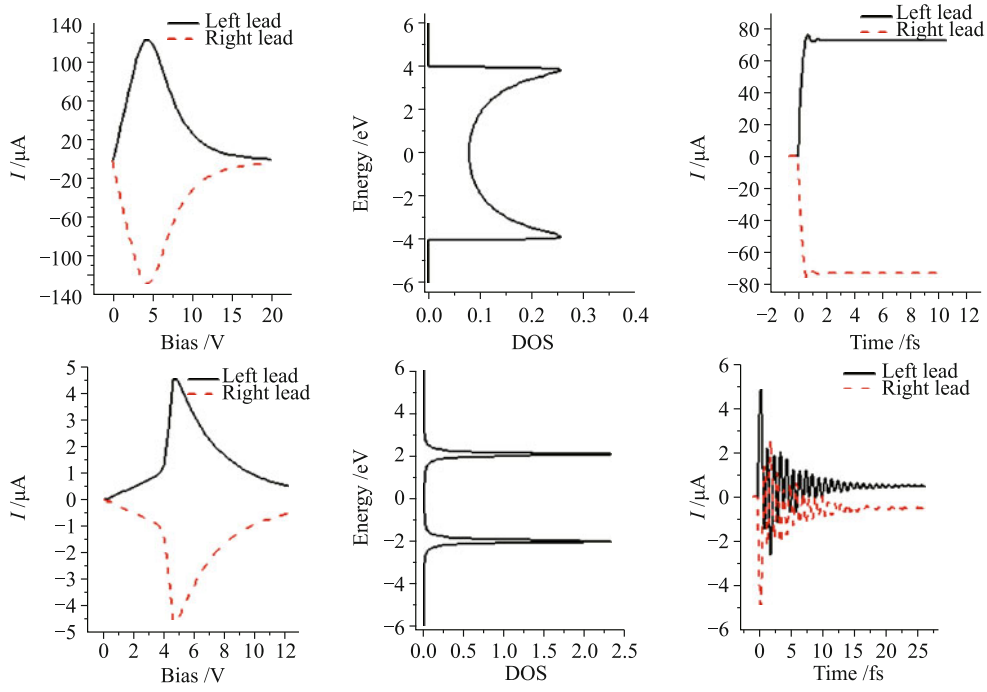

Fig. 4 I–V curve (*left*), DOS spectrum (*middle*) and the transient current (*right*) for a 2-atom device with strong contact (*upper row*) and weak contact (*lower row*). The bias voltage is 2 V and is switched on suddenly as a step function. Reproduced from Ref. [55], Copyright © 2012 AIP Publishing LLC.

amplitude of the oscillation at the beginning can even be much larger than the steady state current. This long lasting oscillation is again due to the long lifetime of electrons in the device, so they oscillate in device with a small damping before reaching a steady state.

6 Wide-band limit approximation

6.1 RSDM based HEOM in WBL approximation

As mentioned previously, solving the time-dependent transport problem without approximation is computationally very expensive, especially for first-principles simulation of realistic systems. The computational complexity of 2nd-tier HEOM lies in the large number of second tier auxiliary density matrix have to be evaluated. In order to simulate the complex system containing hundreds or thousands of atoms, further approximation should be made to reduce the computational complexity. It is shown that the HEOM terminates at the first tier when WBL approximation is adopted [25, 28], and have been implemented with TDDFT and TDDFTB method [28]. Under the WBL approximation, it is assumed that the band-widths of the leads are infinitely large (wide band) and the line-widths are energy-independent, i.e., $\tilde{\boldsymbol{\Lambda}}_\alpha(\epsilon) = \tilde{\boldsymbol{\Lambda}}_\alpha$ [$\tilde{\boldsymbol{\Lambda}}_\alpha(\epsilon)$ defined here is $\tilde{\boldsymbol{\Lambda}}_\alpha(\epsilon) = \boldsymbol{\Lambda}_\alpha(\epsilon)/2$]. In this case, the energy dependent features of the leads are ignored. The self-energy then becomes

$$\boldsymbol{\Sigma}_\alpha^{<,>}(\tau,t) = \pm 2\mathrm{i}\tilde{\boldsymbol{\Lambda}}_\alpha \int \frac{\mathrm{d}\epsilon}{2\pi} f_\alpha^{<,>}(\epsilon) \mathrm{e}^{\mathrm{i}\int_\tau^t [\epsilon+\Delta_\alpha(t_1)]\mathrm{d}t_1} \quad (30)$$

where $\tilde{\boldsymbol{\Lambda}}_\alpha = \pi \sum_{k_\alpha} |\boldsymbol{V}|^2 \delta(\epsilon_f - \epsilon_{k_\alpha})$ is the line-width function evaluated at the Fermi energy ϵ_f of the unbiased system. The Fermi–Dirac distribution function again can be expanded using Padé spectrum decomposition in Eq. (22). For certain system at temperature T, the number of Padé expansion is chosen such that the validity length L, defined by $\delta f(\epsilon)|_{\beta(\epsilon-\mu_\alpha)=L} = \delta$, where δ is the tolerance desired in the simulation and $\delta f(\epsilon)$ is deviation from exact Fermi–Dirac distribution function, is equal to $\beta(\epsilon_{max} + |\mu_\alpha|)$, where ϵ_{max} is the maximum absolute value of the eigenvalues of Fock matrix.

With the Padé expansion and WBL approximation, the time-domain lesser self-energy in Eq. (30) can be evaluated analytically through contour integration and Cauchy's residue theorem, which results in

$$\boldsymbol{\Sigma}_\alpha^{<,>}(\tau,t) \approx \pm\frac{\mathrm{i}}{2}\delta(t-\tau)\tilde{\boldsymbol{\Lambda}}_\alpha + x\sum_k^N \boldsymbol{\Sigma}_{\alpha k}^x(\tau,t) \quad (31)$$

where $x = +$ for $t \geqslant \tau$ and $x = -$ for $t < \tau$, corresponding to upper (+) or lower half plane (−) contour integration. $\boldsymbol{\Sigma}_{\alpha k}^{\pm}(\tau,t)$ is defined as

$$\boldsymbol{\Sigma}_{\alpha k}^{\pm}(\tau,t) = 2R_k \mathrm{e}^{\mathrm{i}\int_\tau^t \tilde{\epsilon}_{\alpha k}^{\pm}(t_1)\mathrm{d}t_1} \tilde{\boldsymbol{\Lambda}}_\alpha \quad (32)$$

where $\tilde{\epsilon}_{\alpha k}^{\pm}(t) = \pm\mathrm{i}z_k + \mu_\alpha + \Delta_\alpha(t)$. The first tier auxiliary density matrix is then evaluated as

$$\begin{aligned}\boldsymbol{\varphi}_\alpha(t) &= \mathrm{i}\int_{-\infty}^t \mathrm{d}\tau[\boldsymbol{G}_D^<(t,\tau)\boldsymbol{\Sigma}_\alpha^>(\tau,t) - \boldsymbol{G}_D^>(t,\tau)\boldsymbol{\Sigma}_\alpha^<(\tau,t)] \\ &= \mathrm{i}[\boldsymbol{\sigma}(t) - 1/2]\boldsymbol{\Lambda}_\alpha + \sum_k^N \boldsymbol{\varphi}_{\alpha k}(t) \quad (33)\end{aligned}$$

The first term on the right hand side (RHS) comes from the integration over $\boldsymbol{G}_D^{>/<}(t,\tau)$ and delta function $\delta(\tau - t)$. The energy-discretized first tier ARSDMs $\boldsymbol{\varphi}_{\alpha k}(t)$ are defined as

$$\boldsymbol{\varphi}_{\alpha k}(t) = -\mathrm{i}\int_{-\infty}^{\infty} \mathrm{d}\tau \boldsymbol{G}^r(t,\tau)\boldsymbol{\Sigma}_{\alpha k}^+(\tau,t) \quad (34)$$

And each of them evolves according to the following EOM, which can be derived easily since the EOMs of $\boldsymbol{G}^r(t,\tau)$ and $\boldsymbol{\Sigma}_{\alpha k}^+(\tau,t)$ are simply linear equations of themselves,

$$\mathrm{i}\dot{\boldsymbol{\varphi}}_{\alpha k}(t) = -2\mathrm{i}R_k\tilde{\boldsymbol{\Lambda}}_\alpha - [\tilde{\epsilon}_{\alpha k}^+(t) - \boldsymbol{h}(t) + \mathrm{i}\tilde{\boldsymbol{\Lambda}}]\boldsymbol{\varphi}_{\alpha k}(t) \quad (35)$$

where $\tilde{\boldsymbol{\Lambda}} = \sum_\alpha \tilde{\boldsymbol{\Lambda}}_\alpha$ is the total line-width function of two leads.

Under the WBL approximation, Eqs. (14), (33) and (35) give us a close set of EOMs, without the need to introduce the second tier auxiliary density matrices, which is termed as the NEGF-HEOM-WBL method. Thus propagating this set of EOMs with proper initial values gives the time-dependent density matrix, auxiliary density matrices, and then the time-dependent quantities of interest are evaluated from them. Since no second tier auxiliary density matrices are required, the WBL approximation is therefore much more desirable in terms of computational time as well as memory requirement for simulating large realistic devices.

For the initial values for the EOMs, at initial time $t = 0$ before switching on the bias voltage, the whole system should be in equilibrium. All quantities are therefore time-independent, so do the RSDM and ARSDMs. By requiring Eqs. (14) and (35) to equal to zero at initial time, the initial conditions are given by

$$\boldsymbol{\sigma}(0) = \frac{1}{2}\boldsymbol{I} + \sum_{\alpha k}\mathrm{Re}\left(\frac{2R_k}{\tilde{\epsilon}_{\alpha k}(0)\boldsymbol{I} - \boldsymbol{h}(0) + \mathrm{i}\tilde{\boldsymbol{\Lambda}}}\right) \quad (36)$$

$$\boldsymbol{\varphi}_{\alpha k}(0) = -\frac{2\mathrm{i}R_k}{\tilde{\epsilon}_{\alpha k}(0)\boldsymbol{I} - \boldsymbol{h}(0) + \mathrm{i}\tilde{\boldsymbol{\Lambda}}}\tilde{\boldsymbol{\Lambda}}_\alpha \quad (37)$$

These two equations provide the initial conditions for the EOMs. After bias voltage is switched on, the device

is driven out of equilibrium and the dynamic response of the device can be obtained by solving the EOMs of $\boldsymbol{\sigma}(t)$ and $\boldsymbol{\varphi}_{\alpha k}(t)$ in time domain.

6.2 TDDFT(B)-NEGF-HEOM-WBL formalism

This NEGF-HEOM-WBL formalism has been implemented in the framework of TDDFT and time-dependent density functional tight-binding (TDDFTB) method, which is called TDDFT(B)-NEGF-HEOM-WBL formalism [28]. In this formalism, the system is assumed to be in its ground state initially, which is determined by molecular cluster based technique [24]. In the ground state calculation, not only the device region but also a portion of the leads have to be included in the extended cluster so that the the periodic diagonal and off-diagonal blocks of lead KS Hamiltonian $\boldsymbol{h}_{LL/RR}$ is extracted from the whole KS Hamiltonian to evaluate the surface Green's function $\boldsymbol{g}_{L/R}$ [58] and extract the device-lead coupling matrix $\boldsymbol{h}_{DL/DR}$ to calculate line-width function $\boldsymbol{\Lambda}_{L/R}$. The initial values for $\boldsymbol{\sigma}_D$ and $\boldsymbol{\varphi}_{\alpha k}$ are then evaluated as described above.

The time propagation of the density matrix $\boldsymbol{\sigma}(t)$ and auxiliary density matrix $\boldsymbol{\varphi}_{\alpha k}(t)$ was carried out with the fourth-order Runge–Kutta (RK4) method. After bias voltage is turned on, The KS Fock matrix changes with time according to the induced electron density. The change in KS Fock matrix comprises of two parts, the induced Hartree potential $V_H(\boldsymbol{r},t)$ and induced XC potential $V_{xc}(\boldsymbol{r},t)$,

$$\boldsymbol{h}(t) = \boldsymbol{h}(0) + \delta\boldsymbol{V}_H(t) + \delta\boldsymbol{V}_{xc}(t) \tag{38}$$

where $\boldsymbol{h}(0)$ is the ground state KS Fock matrix. These two components $\delta\boldsymbol{V}_H(t)$ and $\delta\boldsymbol{V}_{xc}(t)$ have to be updated at each time step according to the induced electron density $\delta n(\boldsymbol{r},t)$, which is a consequence of the voltage applied at the leads.

To obtain them, the induced Hartree and XC potential are first solved in real space followed by projecting them on the basis set. The evaluation of induced XC potential depends on which XC functional we employ and the induced Hartree potential is obtained by solving the Poisson equation:

$$\nabla^2\delta V_H(\boldsymbol{r},t) = -4\pi\delta n(\boldsymbol{r},t) \tag{39}$$

subject to the boundary condition at the lead-device interface:

$$\begin{aligned}\delta V_H(\boldsymbol{r},t)|_{S_L} &= V_L(t)\\ \delta V_H(\boldsymbol{r},t)|_{S_R} &= V_R(t)\end{aligned} \tag{40}$$

where S_L/S_R are the the interfaces between device and leads; $V_{L/R}(t)$ is the bias voltage applied on lead L/R.

Transient current at each time step is obtained from Eq. (16). The most time-consuming part is the propagation of the first tier ARSDMs $\boldsymbol{\varphi}_{\alpha k}$, since there are $2N_k$ $\boldsymbol{\varphi}_{\alpha k}(t)$ matrices to be propagated at each time step. To reduce the computational cost, the sparsity of the line-width function $\boldsymbol{\Lambda}_\alpha$, which is localized on the top left or bottom right corner, was taken into account and only a small block of $\boldsymbol{\Lambda}_\alpha$ and a partial block of $\boldsymbol{\varphi}_{\alpha k}(t)$ were calculated in the numerical implementation. As a result, the computational cost and memory requirement are reduced and simulating large systems is possible with this method.

6.3 First-principles simulation results

The above TDDFT(B)-NEGF-HEOM-WBL method has been applied to simulate in first-principles the ac response of a (5, 5) carbon nanotube(CNT)-based device [28]. As shown in Fig. 5, it comprises of a (5, 5) CNT, which contains 60 carbon atoms, connected to two aluminum leads from left and right. The distance between the CNT and the aluminum lead is 1.5 Å. The device region includes the CNT as well as one unit cell of the aluminum lead on each side. The whole device region thus contains 60 carbon atoms and 32 aluminum atoms.

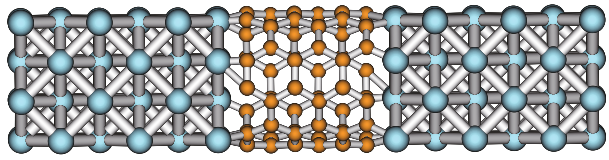

Fig. 5 CNT-based device. There are 60 atoms for the (5, 5) CNT and 16 atoms in a unit cell of aluminum leads. Reproduced from Ref. [28], Copyright © 2013 American Physical Society.

Simulations were done in both TDDFT and TDDFTB levels as shown in Figs. 6 and 7 respectively. Comparison with the AWBL approximation (Ref. [24]) is made. Since the AWBL method is applicable for zero-temperature while the WBL scheme here is not, the WBL simulation is carried out at very low temperatures (5 K in this case) so as to make the comparison meaningful.

The core orbitals are excluded through a projector operator [59] since the core orbitals will play little role in quantum transport. The largest absolute value of the eigenvalues of Fock matrix is found to be around 19 eV after excluding core orbitals. A 300 terms Padé expansion is used for the WBL simulation to achieve tolerance $\delta = 10^{-7}$ for a validity length equal to 4.4×10^4. RK4 propagation with time step equal to 0.015 fs is used. In TDDFT simulation, the minimal basis set STO-3G is employed and the adiabatic localized density

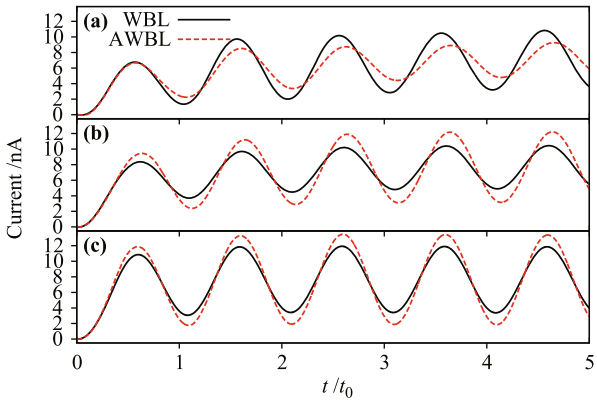

Fig. 6 TDDFT calculation of transient current corresponding to sinusoidal bias voltage, $V(t) = \frac{V_0}{2}(1 - \cos\frac{2\pi t}{t_0})$, $V_0 = 0.1$ meV. **(a)** $t_0 = 2$ fs; **(b)** $t_0 = 5$ fs; **(c)** $t_0 = 10$ fs. The black real line is WBL current; Red dash line is AWBL current. Reproduced from Ref. [28], Copyright © 2013 American Physical Society.

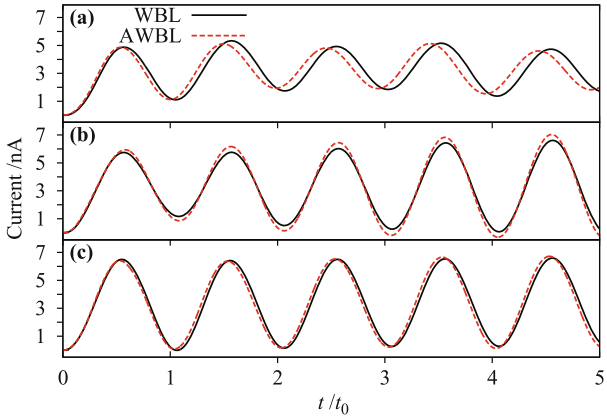

Fig. 7 TDDFTB simulation of transient current corresponding to sinusoidal bias voltage, $V(t) = \frac{V_0}{2}(1 - \cos\frac{2\pi t}{t_0})$, $V_0 = 0.1$ meV. **(a)** $t_0 = 2$ fs; **(b)** $t_0 = 5$ fs; **(c)** $t_0 = 10$ fs. The black real line is WBL current; Red dash line is AWBL current. Reproduced from Ref. [28], Copyright © 2013 American Physical Society.

approximation (ALDA) is chosen as the XC functional. Given the alternating bias voltage, the system is always driven out of steady state. Therefore, the memory effect here plays a more important role than that for exponential growth bias voltage. It can be seen that for both TDDFT and TDDFTB simulations, the AWBL and WBL results agree well with each other under low frequency ac voltage but give different amplitude and phase delays under high frequency bias. This is especially obvious in the case of TDDFTB simulation under the high frequency bias ($t_0 = 2$ fs), in which the AWBL current even leads before the bias voltage. It is thus concluded that the WBL method is more suitable for high frequency simulations whereas the AWBL is good enough for simulation at low frequency.

Finally, a comparison on the steady state current obtained from the TDDFT and static DFT method is made. In present work, the ALDA functional is used in the TDDFT calculation. It is well known that TDDFT with ALDA functional leads to the Landauer–Büttiker formula for the steady state current if it is can be reached in the long-time limit [24, 60]. It has been shown numerically the equivalence between the TDDFT and static DFT result for the steady state current with the adiabatic XC functional even beyond the liner response region [61]. Here, the current obtained from the TDDFT-NEGF-HEOM-WBL is compared with that obtained from the DFT-NEGF-WBL as shown in Fig. 8, which shows the same steady state current. In principle, the inclusion of memory effects beyond the adiabatic approximation will introduce dynamical corrections to the static DFT result for the quantum transport [62–64]. However, the development of accurate functionals for the numerical simulation of quantum transport is not straightforward and still under investigation.

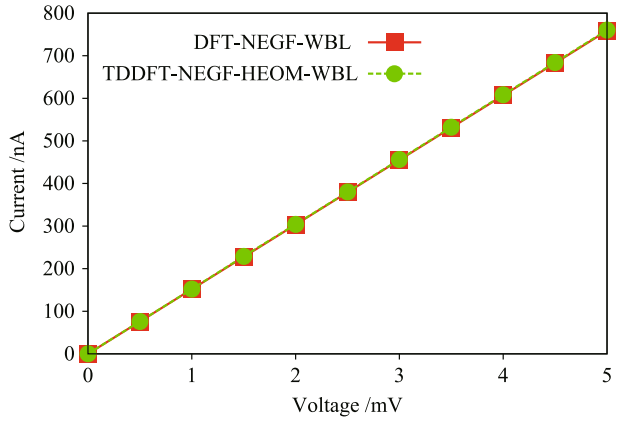

Fig. 8 I–V curves obtained from the TDDFT-NEGF-HEOM-WBL and static DFT-NEGF-WBL method.

7 Concluding remarks

First-principles method for the quantum transport has seen tremendous growth of research interest, however the majority of studies focus on the steady state properties. Besides, the DFT-NEGF method for quantum transport has its theoretical weakness as DFT is a ground state theory and therefore not suitable for non-equilibrium phenomena. Based on the TD-HEDT, the existence of rigorous first-principles method for quantum transport is confirmed. Consequently, an exact formula was developed in terms of HEOM for RSDM and auxiliary density matrices followed by several practical numerical scheme at different levels of approximation as reviewed in this manuscript.

Even though the foundation of TDDFT for quantum transport has been laid, this field is at an early stage

in its development, there are still plenty of rooms for further development and applications. First, the accuracy of TDDFT method for quantum transport is limited by the quality of XC functionals. The XC effect between electrons is intimately related to the quantum transport phenomena [65]. For instance, the discontinuity of XC potential of TDDFT is crucial for the description of coulomb blockade [66]. Currently, ALDA functional is widely used in the implementations of TDDFT for time-dependent quantum transport. However, the importance of the inclusion of memory effects beyond the ALDA has been illustrated [62–64], more efforts have to be paid to the development of accurate XC functionals for quantum transport. A promising attempt is solving Kadanoff–Baym equations by introducing self-energies for electron-electron interaction from many-body perturbation theory (MBPT) [51, 67]. MBPT provides a systematic way for the inclusion of dynmaical XC effects through the selection of proper Feynman diagrams. However, the computational efficiency must be improved before this method is implemented for the simulation of large systems.

Second, previous studies in the TDDFT for quantum transport did not consider the dissipation due to electron-phonon scattering. The inelastic effect due to electron-phonon scattering can play a vital role in the functionality and stability of current-carrying devices. Recent advance has been achieved by the development of dissipative time-dependent quantum transport theory [68], it can be readily combined with TDDFT even through it is currently only implemented on model systems. Future works of TDDFT for quantum transport may also combine the first-principles methods with this dissipative time-dependent quantum transport theory to investigate the dissipative effect due to electron-phonon interaction on transient phenomenon.

Acknowledgements Support from the Hong Kong Research Grant Council (Contracts No. HKU7009/09P, No. 7009/12P, No. 7007/11P, and No. HKUST9/CRF/11G), and the University Grant Council (Contract No. AoE/P-04/08) is gratefully acknowledged.

References

1. M. Auf der Maur, M. Povolotskyi, F. Sacconi, A. Pecchia, G. Romano, G. Penazzi, and A. Di Carlo, TiberCAD: Towards multiscale simulation of optoelectronic devices, *Opt. Quantum Electron.*, 2008, 40(14–15): 1077
2. M. C. Petty, Molecular Electronics: From Principles to Practice, Wiley, 2008: 544
3. A. Aviram and M. A. Ratner, Molecular rectifiers, *Chem. Phys. Lett.*, 1974, 29(2): 277
4. M. A. Reed, C. Zhou, C. J. Muller, T. P. Burgin, and J. M. Tour, Conductance of a molecular junction, *Science*, 1997, 278(5336): 252
5. H. Song, Y. Kim, Y. H. Jang, H. Jeong, M. A. Reed, and T. Lee, Observation of molecular orbital gating, *Nature*, 2009, 462(7276): 1039
6. H. Song, M. A. Reed, and T. Lee, Single molecule electronic devices, *Adv. Mater.*, 2011, 23(14): 1583
7. S. W. Wu, N. Ogawa, and W. Ho, Atomic-scale coupling of photons to single-molecule junctions, *Science*, 2006, 312(5778): 1362
8. M. Galperin, and A. Nitzan, Molecular optoelectronics: the interaction of molecular conduction junctions with light, *Phys. Chem. Chem. Phys.*, 2012, 14(26): 9421
9. A. Nitzan and M. A. Ratner, Electron transport in molecular wire junctions, *Science*, 2003, 300(5624): 1384
10. M. Paulsson, T. Frederiksen, and M. Brandbyge, Inelastic transport through molecules: Comparing first-principles calculations to experiments, *Nano Lett.*, 2006, 6(2): 258
11. M. Galperin, M. A Ratner, and A. Nitzan, Molecular transport junctions: Vibrational effects, *J. Phys.: Condens. Matter*, 2007, 19(10): 103201
12. J. C. Cuevas and E. Scheer, Molecular Electronics: An Introduction to Theory and Experiment, Vol. 1, World Scientific Series in Nanotechnology and Nanoscience, 2010: 703
13. T. Fujisawa, D. G. Austing, Y. Tokura, Y. Hirayama, and S. Tarucha, Electrical pulse measurement, inelastic relaxation, and non-equilibrium transport in a quantum dot, *J. Phys.: Condens. Matter*, 2003, 15: R1395
14. J. Taylor, H. Guo, and J. Wang, Ab initio modeling of quantum transport properties of molecular electronic devices, *Phys. Rev. B*, 2001, 63(24): 245407
15. M. Brandbyge, J. L. Mozos, P. Ordejón, J. Taylor, and K. Stokbro, Density-functional method for nonequilibrium electron transport, *Phys. Rev. B*, 2002, 65(16): 165401
16. M. Elstner, D. Porezag, G. Jungnickel, J. Elsner, M. Haugk, T. Frauenheim, S. Suhai, and G. Seifert, Self-consistent-charge density-functional tight-binding method for simulations of complex materials properties, *Phys. Rev. B*, 1998, 58(11): 7260
17. T. A. Niehaus, S. Suhai, F. Della Sala, P. Lugli, M. Elstner, G. Seifert, and T. Frauenheim, Tight-binding approach to time-dependent density-functional response theory, *Phys. Rev. B*, 2001, 63(8): 085108
18. C. Yam, L. Meng, G. H. Chen, Q. Chen, and N. Wong, Multiscale quantum mechanics/electromagnetics simulation for electronic devices, *Phys. Chem. Chem. Phys.*, 2011, 13(32): 14365
19. L. Meng, C. Yam, S. Koo, Q. Chen, N. Wong, and G. H. Chen, Dynamic multiscale quantum mechanics/electromagnetics simulation method, *J. Chem. Theory Comput.*, 2012, 8(4): 1190

20. G. Stefanucci and C. O. Almbladh, Time-dependent quantum transport: An exact formulation based on TDDFT, *Europhys. Lett.*, 2004, 67(1): 14
21. J. Maciejko, J. Wang, and H. Guo, Time-dependent quantum transport far from equilibrium: An exact nonlinear response theory, *Phys. Rev. B*, 2006, 74(8): 085324
22. S. Kurth, G. Stefanucci, C. O. Almbladh, A. Rubio, and E. K. U. Gross, Time-dependent quantum transport: A practical scheme using density functional theory, *Phys. Rev. B*, 2005, 72(3): 035308
23. J. Yuen-Zhou, D. G. Tempel, C. A. Rodríguez-Rosario, and A. Aspuru-Guzik, Time-dependent density functional theory for open quantum systems with unitary propagation, *Phys. Rev. Lett.*, 2010, 104(4): 043001
24. X. Zheng, F. Wang, C. Y. Yam, Y. Mo, and G. H. Chen, Time-dependent density-functional theory for open systems, *Phys. Rev. B*, 2007, 75(19): 195127
25. X. Zheng, G. H. Chen, Y. Mo, S. Koo, H. Tian, C. Yam, and Y. Yan, Time-dependent density functional theory for quantum transport, *J. Chem. Phys.*, 2010, 133(11): 114101
26. S. H. Ke, R. Liu, W. Yang, and H. U. Baranger, Time-dependent transport through molecular junctions, *J. Chem. Phys.*, 2010, 132(23): 234105
27. K. Burke, R. Car, and R. Gebauer, Density functional theory of the electrical conductivity of molecular devices, *Phys. Rev. Lett.*, 2005, 94(14): 146803
28. Y. Zhang, S. Chen, and G. H. Chen, First-principles time-dependent quantum transport theory, *Phys. Rev. B*, 2013, 87(8): 085110
29. S. Chen, H. Xie, Y. Zhang, X. Cui, and G. H. Chen, Quantum transport through an array of quantum dots, *Nanoscale*, 2013, 5(1): 169
30. A. P. Jauho, N. S. Wingreen, and Y. Meir, Time-dependent transport in interacting and noninteracting resonant-tunneling systems, *Phys. Rev. B*, 1994, 50(8): 5528
31. C. Y. Yam, Y. Mo, F. Wang, X. B. Li, G. H. Chen, X. Zheng, Y. Matsuda, J. Tahir-Kheli, and W. A. Goddard III, Dynamic admittance of carbon nanotube-based molecular electronic devices and their equivalent electric circuit, *Nanotechnology*, 2008, 19(49): 495203
32. K. F. Albrecht, H. Wang, L. Mühlbacher, M. Thoss, and A. Komnik, Bistability signatures in nonequilibrium charge transport through molecular quantum dots, *Phys. Rev. B*, 2012, 86(8): 081412
33. E. Khosravi, S. Kurth, G. Stefanucci, and E. Gross, The role of bound states in time-dependent quantum transport, *Appl. Phys. A*, 2008, 93(2): 355
34. E. Khosravi, G. Stefanucci, S. Kurth, and E. K. Gross, Bound states in time-dependent quantum transport: Oscillations and memory effects in current and density, *Phys. Chem. Chem. Phys.*, 2009, 11(22): 4535
35. B. Popescu, P. B. Woiczikowski, M. Elstner, and U. Kleinekathöfer, Time-dependent view of sequential transport through molecules with rapidly fluctuating bridges, *Phys. Rev. Lett.*, 2012, 109(17): 176802
36. J. K. Tomfohr and O. F. Sankey, Time-dependent simulation of conduction through a molecule, *physica status solidi (b)*, 2001, 226(1): 115
37. N. Bushong, N. Sai, and M. Di Ventra, Approach to steady-state transport in nanoscale conductors, *Nano Lett.*, 2005, 5(12): 2569
38. J. Muga, J. Palao, B. Navarro, and I. Egusquiza, Complex absorbing potentials, *Phys. Rep.*, 2004, 395(6): 357
39. R. Baer, T. Seideman, S. Ilani, and D. Neuhauser, Ab initio study of the alternating current impedance of a molecular junction, *J. Chem. Phys.*, 2004, 120(7): 3387
40. P. Hohenberg and W. Kohn, Inhomogeneous electron gas, *Phys. Rev.*, 1964, 136(3B): B864
41. E. Runge and E. K. U. Gross, Density-functional theory for time-dependent systems, *Phys. Rev. Lett.*, 1984, 52(12): 997
42. S. Fournais, M. Hoffmann-Ostenhof, T. Hoffmann-Ostenhof, and T. Østergaard Sørensen, Analyticity of the density of electronic wavefunctions, *Arkiv för Matematik*, 2004, 42(1): 87
43. S. Fournais, M. Hoffmann-Ostenhof, T. Hoffmann-Ostenhof, and T. Østergaard Sørensen, The electron density is smooth away from the nuclei, *Commun. Math. Phys.*, 2002, 228(3): 401
44. X. Zheng, C. Yam, F. Wang, and G. H. Chen, Existence of time-dependent density-functional theory for open electronic systems: Time-dependent holographic electron density theorem, *Phys. Chem. Chem. Phys.*, 2011, 13(32): 14358
45. G. Vignale and W. Kohn, Current-dependent exchange-correlation potential for dynamical linear response theory, *Phys. Rev. Lett.*, 1996, 77(10): 2037
46. M. Di Ventra and R. D'Agosta, Stochastic time-dependent current-density-functional theory, *Phys. Rev. Lett.*, 2007, 98(22): 226403
47. R. D'Agosta and M. Di Ventra, Stochastic time-dependent current-density-functional theory: A functional theory of open quantum systems, *Phys. Rev. B*, 2008, 78(16): 165105
48. M. Galperin and S. Tretiak, Linear optical response of current-carrying molecular junction: a nonequilibrium Green's function-time-dependent density functional theory approach, *J. Chem. Phys.*, 2008, 128(12): 124705
49. Y. Xing, B. Wang, and J. Wang, First-principles investigation of dynamical properties of molecular devices under a steplike pulse, *Phys. Rev. B*, 2010, 82(20): 205112
50. L. Zhang, Y. Xing, and J. Wang, First-principles investigation of transient dynamics of molecular devices, *Phys. Rev. B*, 2012, 86(15): 155438
51. P. Myöhänen, A. Stan, G. Stefanucci, and R. van Leeuwen, Kadanoff–Baym approach to quantum transport through interacting nanoscale systems: From the transient to the steady-state regime, *Phys. Rev. B*, 2009, 80(11): 115107

52. R. Gebauer, K. Burke, and R. Car, in: Time-Dependent Density Functional Theory, Lecture Notes in Physics, Vol. 706, edited by M. Marques, C. Ullrich, F. Nogueira, A. Rubio, K. Burke, and E. U. Gross, Berlin Heidelberg: Springer, 2006: 463–477
53. J. Jin, X. Zheng, and Y. Yan, Exact dynamics of dissipative electronic systems and quantum transport: Hierarchical equations of motion approach, *J. Chem. Phys.*, 2008, 128(23): 234703
54. H. Tian and G. H. Chen, An efficient solution of Liouville-von Neumann equation that is applicable to zero and finite temperatures, *J. Chem. Phys.*, 2012, 137(20): 204114
55. H. Xie, F. Jiang, H. Tian, X. Zheng, Y. Kwok, S. Chen, C. Yam, Y. Yan, and G. H. Chen, Time-dependent quantum transport: an efficient method based on Liouville–von-Neumann equation for single-electron density matrix, *J. Chem. Phys.*, 2012, 137(4): 044113
56. J. Hu, R. X. Xu, and Y. Yan, Communication: Padé spectrum decomposition of Fermi function and Bose function, *J. Chem. Phys.*, 2010, 133(10): 101106
57. J. R. Soderstrom, D. H. Chow, and T. C. McGill, New negative differential resistance device based on resonant interband tunneling, *Appl. Phys. Lett.*, 1989, 55(11): 1094
58. M. P. L. Sancho, J. M. L. Sancho, J. M. L. Sancho, and J. Rubio, Highly convergent schemes for the calculation of bulk and surface Green functions, *J. Phys. F*, 1985, 15(4): 851
59. F. Wang, C. Y. Yam, G. H. Chen, and K. Fan, Density matrix based time-dependent density functional theory and the solution of its linear response in real time domain, *J. Chem. Phys.*, 2007, 126(13): 134104
60. G. Stefanucci, S. Kurth, E. Gross, and A. Rubio, in: Molecular and Nano Electronics: Analysis, Design and Simulation, Theoretical and Computational Chemistry, Vol. 17, edited by J. Seminario, Elsevier, 2007: 247–284
61. C. Yam, X. Zheng, G. Chen, Y. Wang, T. Frauenheim, and T. A. Niehaus, Time-dependent versus static quantum transport simulations beyond linear response, *Phys. Rev. B*, 2011, 83(24): 245448
62. N. Sai, M. Zwolak, G. Vignale, and M. Di Ventra, Dynamical corrections to the DFT-LDA electron conductance in nanoscale systems, *Phys. Rev. Lett.*, 2005, 94(18): 186810
63. F. Evers, F. Weigend, and M. Koentopp, Conductance of molecular wires and transport calculations based on density-functional theory, *Phys. Rev. B*, 2004, 69(23): 235411
64. G. Stefanucci and S. Kurth, Towards a description of the Kondo effect using time-dependent density-functional theory, *Phys. Rev. Lett.*, 2011, 107(21): 216401
65. E. Khosravi, A. M. Uimonen, A. Stan, G. Stefanucci, S. Kurth, R. van Leeuwen, and E. K. U. Gross, Correlation effects in bistability at the nanoscale: Steady state and beyond, *Phys. Rev. B*, 2012, 85(7): 075103
66. S. Kurth, G. Stefanucci, E. Khosravi, C. Verdozzi, and E. K. U. Gross, Dynamical Coulomb blockade and the derivative discontinuity of time-dependent density functional theory, *Phys. Rev. Lett.*, 2010, 104(23): 236801
67. P. Myöhänen, A. Stan, G. Stefanucci, and R. van Leeuwen, A many-body approach to quantum transport dynamics: Initial correlations and memory effects, *Europhys. Lett.*, 2008, 84(6): 67001
68. Y. Zhang, C. Y. Yam, and G. H. Chen, Dissipative time-dependent quantum transport theory, *J. Chem. Phys.*, 2013, 138(16): 164121